CHAPTER V

Gold nanoparticles (AuNPs) modified surface of PEDOT doped with graphene oxide (GO) and its application for the detection of Aflatoxin B_1 and Organophosphate

This chapter deals with the morphological, structural and electro-catalytic of PEDOT-GO/GCE, AuNPs/PEDOT-GO/GCE, BSA/anti-AFB_1/AuNPs/PEDOT-GO/GCE and AChE/AuNPs/PEDOT-GO/GCE. The electrochemical properties of the synthesized electrodes have been done using cyclic voltammetry and electrochemical impedance spectroscopy. A comparative study of all modified electrodes has been done and AuNPs/PEDOT-GO/GCE has been used as a matrix to immobilize anti-AFB_1 and AChE. The Sensing of the bioelectrode towards the respective analytes has been done and the different sensing parameters, viz. linearity, sensitivity, incubation time, limit of detection and limit of quantification have been determined.

5.1 Introduction

Inexpensive immunosensors have been long pursued to detect AFB_1 for food quality screening but the sensitivity is far from satisfactory. In this regard, cost-effective portable biosensors for efficient detection of AFB_1 with high sensitivity and selectivity are required [373]. Similarly, in the past decades enormous effort have been made viz. self-assembled monolayers, gel based biosensors, graphene based biosensors, metal and metal oxide based biosensors to develop efficient and simple methods to determine organophosphate levels [374, 375]. Numerous enzymes immobilized electrochemical biosensors based on different nanocomposites of metal nanoparticles [376], carbon compounds [377], ionic liquids [378] and biopolymers [379] have been fabricated and emerged as a powerful tool to detect organophosphates. However, most of the reported AChE inhibition electrochemical biosensors still face serious instability problems [380].

The introduction of a thin PEDOT film increases the effective surface area of the electrode substrate without sacrificing the conductive property of the electrode [381]. Moreover, it can easily be functionalized with negatively charged dopants like GO [382], functionalized CNTs [383], PSS [384] and metal nanoparticles [376] as the electro-polymerization of the monomer results in positively charged polymer backbone [385]. The hydrophobic nature and the absence of functional groups such as -COOH & $-NH_2$ of this polymer may hinder its application in biosensors [386].

In the present thesis work, *in situ* incorporation of GO in PEDOT layers has been carried out in order to get a hydrophilic surface with free functional groups for covalent binding with antibodies and the composite is formed by π-π stacking between the GO layers and polymer rings [387]. Poly (3, 4-ethylene dioxythiophene) (PEDOT) and GO based composite has been developed by controllable electro-polymerization of monomer EDOT in presence of GO by the application of potential [388] and it has been used in biological and biomedical areas such as biosensors and bio-interfaces [389, 390]. It has been reported that a highly efficient antibody or enzyme electrode can be obtained by covalent attachment of carboxyl group of GO with the amine groups of the proteins [391, 392]. It has been reported that the conductivity of PEDOT can be dramatically increased after incorporation of graphene oxide (GO) [393]. However, a GO based biosensor has sensitivity much lower than that of a graphene-based biosensor due to its poor conductivity [393]. In order to improve the sensitivity of the PEDOT-GO composite based electrodes, gold nanoparticles (AuNPs) have been deposited. Spherical gold nanoparticles (AuNPs) of 5nm to 100 nm size have drawn significant attention in the construction of immunosensors due to their high conductivity and improved immobilization ability [394, 395]. AuNPs help in better immobilization of the protein molecules providing native microenvironment thereby retaining their activity and preventing them from leaching back into the bulk solution [396]. Although both PEDOT and GO are good substrate for depositing AuNPs to fabricate an efficient immunosensor, the loading of Au-NPs onto the composites has been done for the first time. The synergistic effect of all the components may provide an excellent platform for immobilization of anti-AFB_1 and AChE with improved analytical parameters.

In chapter 4, the efficiency of the AuNPs/PEDOT/GCE towards the detection of AFB_1 has been discussed and an excellent sensitivity of 0.725 $\mu Ang^{-1}mL$ in a

linear range of 0.5 to 20 ng/mL with LOD value of 0.0308 ng/mL. Moreover the activity of AChE immobilized in AuNPs/PEDOT/GCE retains its activity and showed a good catalytic behavior towards thiocholine with K_m value of 0.83 mM. In this present thesis chapter the functionalization of PEDOT with GO and AuNPs has been done with a view to enhance the sensitivity towards the detection of AFB_1 and Methyl parathion (MP). We have achieved a better sensitivity of 0.998 $\mu Ang^{-1}mL$ towards AFB_1 detection within a linear range of 0.5 to 20 ng/mL and the affinity of the immobilized AChE towards hydrolysis of AThCl is enhanced with K_m value of 0.2 mM.

In this study we have explored a sensitive and stable electrochemical sensing strategy for highly efficient and rapid detection of AFB1 and MP. The electrode has been synthesized by two-step procedure (i) electrochemical polymerization of EDOT in presence GO as dopant, (ii) deposition of AuNPs by electrochemical reduction of auric chloride onto the modified GCE.

Morphological studies were carried out by Field emission Scanning Electron Microscope (JEOL-JSM-6390LV). Contact angle measurements were made by Degree of Hydrophilicity measurement set up (Model: DSA 15B). The FT-IR spectrum (Spectrum 100 with software version CPU32) was used for the conformational studies. All the electrochemical measurements, viz. cyclic voltammetry, impedance spectroscopy and Differential pulse voltammetry were performed using a Potentiostat/Galvanostat/ZRA (Gamry Reference 3000, USA) with Gamry Echem Analyst Software. Glassy carbon electrode, Ag/AgCl (3 M KCl) and a platinum wire were used as working, reference and auxiliary electrodes, respectively. The cyclic voltammetry and impedance spectroscopy measurements were performed in 100mM PBS containing 5mM $K_3[Fe(CN)_6]$ / $K_4[Fe(CN)_6]$ keeping 1:1 ratio as redox probe. The impedance spectra were measured in the frequency range from 10^6 Hz to 0.08 Hz at amplitude of 20mV vs. Ag/AgCl. The activity of BSA/anti-AFB_1/AuNPs/PEDOT-GO/GCE and AChE/AuNPs/PEDOT-GO/GCE electrodes towards respective analytes has been investigated using DPV technique.

5.2 *Morphological Analysis:*

The FESEM micrograph of PEDOT-GO/GCE depicting a wrinkled petal like graphene oxide distributed randomly with sharp edges is shown in Figure 5.1 (A). The image demonstrates a rough film surface though less agglomerated which may be due to incorporation of GO in the conducting polymer with individual sheet thickness in the range of 12.43 nm to 17.08 nm. Figure 5.1 (B) displays the electrochemically deposited uniform distribution of spherical AuNPs of size ca. 56 nm. The PEDOT-GO composite not only provides a large surface area for the deposition of AuNPs but also gives a stable surface which resists the agglomeration between the particles. Since it is a layer by layer electrochemical deposition the petal like shape of GO disappears and spherical AuNPs are distributed over the surface.

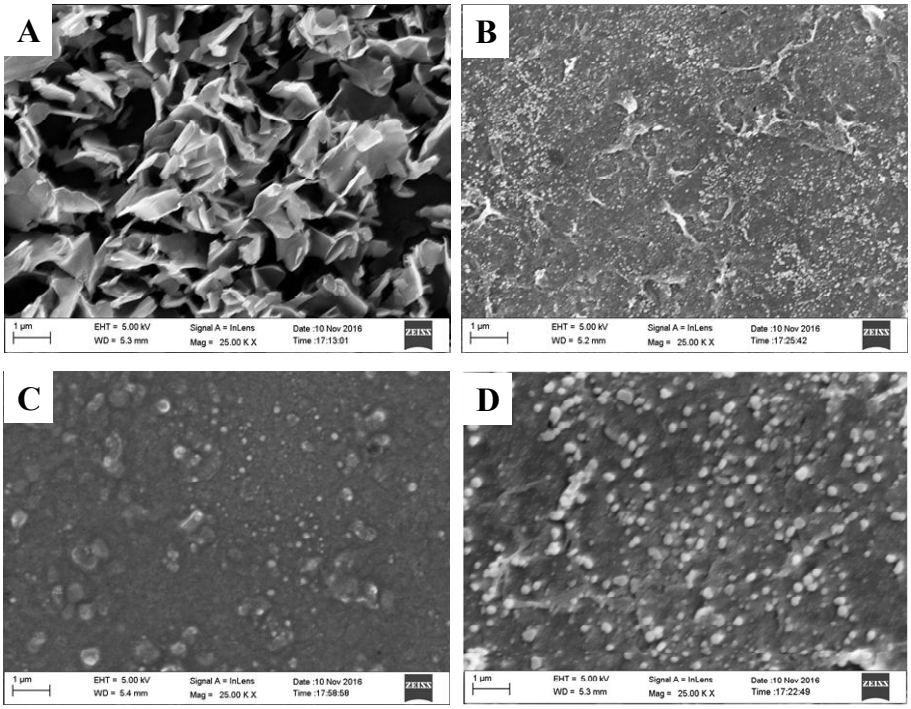

Figure 5.1: FESEM Micrograph of (A) PEDOT-GO film, (B) AuNP/PEDOT-GO film, (C) BSA/anti-AFB_1/AuNPs/PEDOT-GO film and AChE/AuNPs/PEDOT-GO film.

After immobilization of anti-AFB_1 and AChE, the image the layered surface of the film becomes fuzzy as shown in Figure 5.1 (C & D) making the GO sheets and AuNPs close to the interface indistinguishable demonstrating successful

immobilization of antibodies and enzyme onto the AuNPs/PEDOT-GO/GCE surface.

5.3 Contact angle Measurements:

Contact angle (CA) is a measure of static hydrophobicity or hydrophilicity of a matrix and the surface characteristic of the synthesized film using contact angle measurements before immobilization have been done. Figure 5.2 shows contact angle of PEDOT-GO/GCE and AuNPs/PEDOT-GO/GCE. The values of contact angle are found to be less than 90^0 which are characteristic of hydrophilic nature of the film [397].The hydrophilic nature of GO and functionalization of PEDOT-GO/GCE matrix with Au-NPs result in decrease in contact angle making the film more suitable for anti-AFB_1 and AChE immobilization. The water droplet decreases more in volume in case of AuNPs/PEDOT-GO as a result of which the contact angle decreases from 63^0 to 22^0. It implies that the interaction of hydrophilic molecule of the AuNPs/PEDOT-GO film with water is thermodynamically favorable. The antibody immobilization requires a hydrophilic surface since the protein loses its β-sheets configuration at hydrophobic surfaces, confirming a general trend in structural change. The hydrophobicity of surface contributes to unwanted interactions between the proteins and the matrix, which could create a problem with unspecific binding [355].

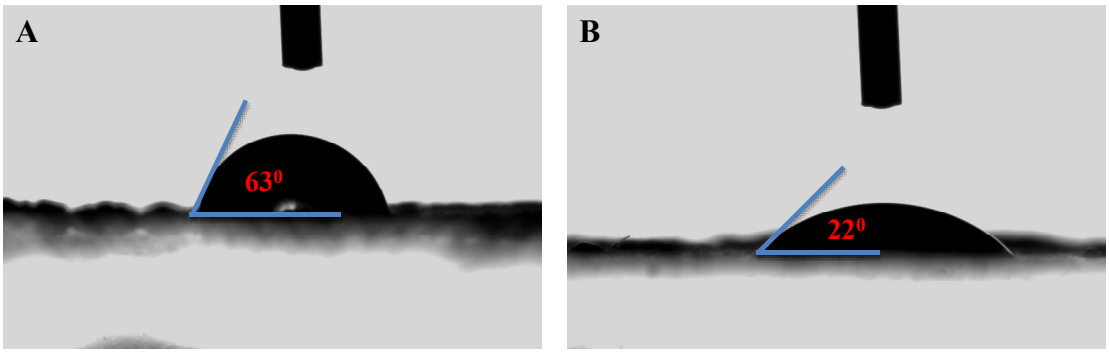

Figure 5.2: Contact angle measurement of (A) PEDOT-GO and (B) AuNPs/PEDOT-GO film.

5.4 FTIR Spectroscopy:

The FTIR spectra of the synthesized PEDOT-GO, AuNPs/PEDOT-GO, BSA/anti-AFB_1/AuNPs/PEDOT-GO and AChE/AuNPs/PEDOT-GO are shown in Figure 5.3. The vibrational bands observed around 1398 and 1510 cm^{-1} correspond to the C–C

and C=C stretching of the thiophene ring respectively. The vibration bands at 1199 and 1080 cm^{-1} are due to the C–O–C bond stretching in the ethylenedioxy group. The absorption bands at 830 and 670 cm^{-1} are assigned to thiophene C–S bond stretching The absorption bands at 852 and 676 cm^{-1} are assigned to thiophene C–S bond stretching and bending vibrations respectively [398]. The band at around 914 cm^{-1} is due to the ethylene dioxy ring deformation mode [399-401].The vibrational band at 3451 cm^{-1} is attributed to the O–H stretching. Various oxygen configurations in the PEDOT-GO structure include the vibration modes of epoxide (C–O–C) (1331 cm^{-1}), sp^2 hybrided C=C (1631 cm^{-1}), in-plane vibrations .The vibration band observed in the wavenumber range of 2800–3000 cm^{-1} is assigned to the C–H stretching mode [402]. The C–O stretching of alkoxy group at 1510 cm^{-1} and O–H stretching peak at 3451 cm^{-1} provide evidence that several types of functional groups are indeed generated by oxidation [403, 404]. The absorption peak at 1765 cm^{-1} is usually associated with the doped state of PEDOT [356]. In the case of AuNPs functionalized polymer matrix, the intensity increases due to the doping of AuNPs within the polymer matrix [356].

For BSA/anti-AFB_1/AuNPs/PEDOT-GO/GCE and AChE/AuNPs/PEDOT-GO/GCE, the amide I band at 1630 cm^{-1}, amide II band at 1534 cm^{-1} and 1379 cm^{-1} demonstrate immobilization of antibodies and enzyme [405, 406] onto the AuNPs functionalized PEDOT-GO composite film.

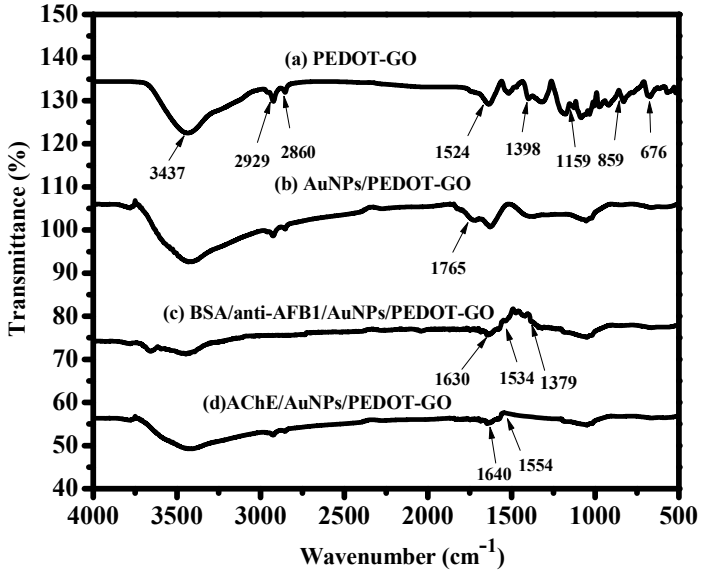

Figure 5.3: FTIR spectra of (a) PEDOT-GO/GCE, (b) AuNP/PEDOT-GO/GCE, (c) BSA/anti-AFB_1/AuNPs/PEDOT-GO/GCE and (d) AChE/AuNPs/PEDOT-GO/GCE.

5.5 Electrochemical Impedance Spectroscopy:

The electron transfer properties of the electrode have been characterized by EIS, an effective method for probing the features of the electrode after different surface modifications [360]. The equivalent circuit, made up of dissipative component resistor and storage component capacitor which represents barrier when current flows between working electrode and the counter electrode, is shown in Scheme 4.1. It is the study of complex impedance represented as the sum of the real (Z') and imaginary ($-Z''$) components [$Z = Z' + j\,(-Z'')$, where $j = \sqrt{-1}$] with Φ (the phase angle) = $\tan^{-1}$ [$Z''(\omega)/Z'(\omega)$] [360] where

$$Z(\omega) = R_s + \frac{R_p}{1+\omega^2 R_p^2 C_d^2} - j\frac{\omega R_p^2 C_d}{1+\omega^2 R_p^2 C_d^2} = Z'(\omega) - j\,Z'' \quad (5.1)$$

at high frequencies $\omega \to \infty$. At low frequencies ($\omega \to 0$), it becomes

$$Z(\omega) = R_s + R_p + \sigma\omega^{-1/2} - j\left(\sigma\omega^{-1/2} + 2\sigma^2 C_d\right) \quad (5.2)$$

The Warburg impedance is related to σ by the equation:

$$Z_w = \left(\frac{2}{\omega}\right)^{1/2}\sigma \quad (5.3)$$

where, R_s is the ohmic resistance of the solution between working electrode and the counter electrode and R_p is the polarization resistance. At zero potential R_p can be described as the resistance of electron transfer (R_{et}) at the electrode-electrolyte interface. Figure 5.4 (A) shows the parametric plot of frequency response of impedance called Nyquist plot which includes a semicircle portion and a linear portion, with the former at higher frequencies corresponding to the electron transfer limited process and the latter at lower frequencies corresponding to the diffusion process. The semicircle diameter of well conducting substrates equals to the electron transfer resistance (R_{et}). Generally, the R_{et} is an index to represent the electro-catalytic activity of the electrodes, the smaller R_{et} corresponds to the less overpotential required for the electron transferring from an electrode to the electrolyte [407].

The calculated impedance parameters from Nyquist plot, Bode plot and phase shift plot are tabulated in Table 5.1. The generated data shows that the R_{et} value of PEDOT-GO/GCE is smaller than that of bare GCE which clearly depicts that a layer of PEDOT-GO composite is formed and promotes charge transfer [394]. The

deposition of AuNPs over the composite film results in remarkable decrease in R_{et}. The R_{et} value increases in the order AuNPs/PEDOT-GO/GCE < PEDOT-GO/GCE < GCE < AChE/PEDOT-GO/GCE < BSA/anti-AFB_1/PEDOT-GO/GCE, which indicates reverse order of electro-catalytic behavior. The C_{dl} values have been calculated using the relationship between the frequency (f_{max}) associated with maximum value of Z'' (ω) and charge transfer resistance R_{et} given by equation (5.4):

$$C_{dl} = \frac{1}{2\pi f_{max} R_{et}} \tag{5.4}$$

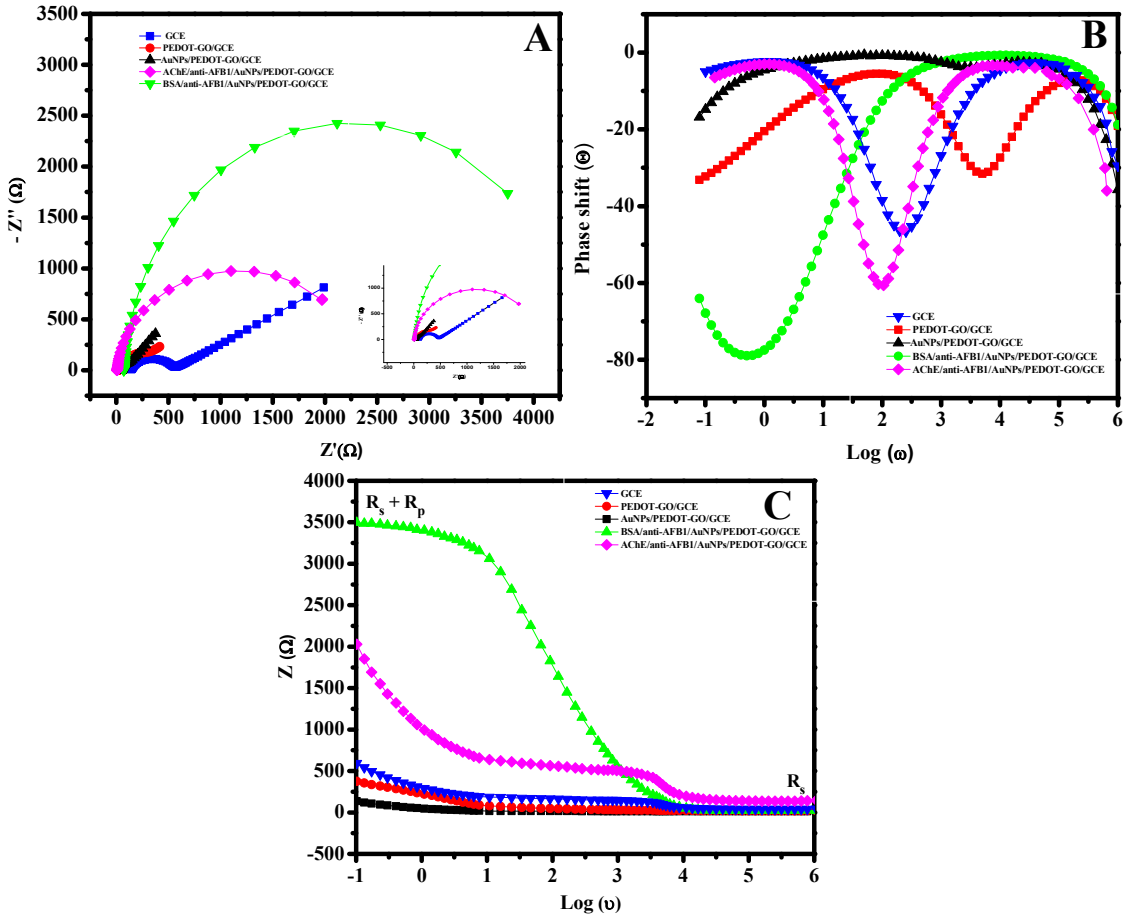

Figure 5.4 : EIS pattern of all modified electrodes (A) Nyquist Plot (Z′ vs. -Z″), (B) Bode plot (Z vs. Log ω) and (C) Phase shifts in 100mM PBS and 5mM $[Fe(CN)_6]^{3-/4-}$.

The C_{dl} value is increased after modification of GCE with PEDOT-GO (Table 5.1) which may be attributed to the capacitive behavior of GO as it also exhibits a high specific surface area that results in the large electrical double-layer [408]. The value of C_{dl} is maximum for BSA/anti-AFB_1/PEDOT-GO/GCE and

AChE/AuNPs/PEDOT-GO/GCE with phase angle of 78.4^0 and 60^0 indicating that the electrode has became more capacitive after immobilization of anti-AFB_1 and AChE which are non-conducting in nature. It implies more accumulation of charges in the interface of these electrodes which hinders the flow of electron between working electrode and the electrolyte which is accordance to the results of cyclic voltammetry.

Table 5.1: The calculated value of R_{et}, C_{dl} and Φ for the modified electrodes.

Electrode	$R_{et}(\Omega)$	C_{dl} (F)	Φ (degree)
GCE	483.92	1.13×10^{-4}	45
PEDOT-GO/GCE	225	1.19×10^{-6}	38
AuNPs/PEDOT-GO/GCE	105	3.42×10^{-7}	11
BSA/anti-AFB_1/AuNPs/PEDOT-GO/GCE	3709	2.03×10^{-3}	78.4
AChE/AuNPs/PEDOT-GO/GCE	1974	7.9×10^{-4}	59.3

5.6 Cyclic Voltammetry Studies:

5.6.1 Electrocatalytic behavior of modified electrodes towards redox species:

Cyclic Voltammetry (CV) of bare and modified GCE has been conducted to understand the electro-active nature of various composites on the electrode. Figure 5.5 (A) shows the CV of the GCE, PEDOT/GCE and AuNPs/PEDOT-GO/GCE in 100 mM PBS (pH 7.4) solution, which shows are no existence of any measurable peaks. The area of the CV curve becomes larger after the electro-polymerization of PEDOT-GO onto the GCE surface, which may be attributed to the favorable capacitance and conductivity of PEDOT-GO composites [394, 408]. While two reduction peaks at 0.45 V and 0.546 V appeared for AuNPs/PEDOT-GO/GCE, corresponding to the reduction reactions of Au(3+)→Au(+) and Au(+)→Au(0), implying that Au nanoparticles are successfully deposited on the surface of the PEDOT-GO film [409, 410] . Figure 5.5 (B) shows the cyclic voltammogram (CV) of (a) GCE, (b) PEDOT-GO/GCE, (c) AuNPs/PEDOT-GO/GCE in a solution

containing 100mM PBS (pH 7.4) and 5.0 mM $[Fe(CN)_6]^{3-/4-}$ as a redox probe at a scan rate of 5 mV s^{-1}. All the modified electrodes offers a well-defined quasi-reversible redox behavior (curve a), which is attributed to a high level of electron transfer between $[Fe(CN)_6]^{3-/4-}$ solution and the electrode [Fe(IV) ↔ Fe(III) + e']. The electro-catalytic properties of all the electrodes depends on two factor (i) the peak oxidation (I_{pa}) and reduction current (I_{pc}) of [Fe(IV)/Fe(III)] system and (ii) the peak to peak separation (ΔE_p) [410-413]. Scheme 5.1 shows the possible mechanism of electro-catalytic behavior of the modified electrode. The high peak current value suggests an enhanced redox behavior to Fe(IV)/Fe(III), and the ΔE_p value depends not only on the standard electrochemical rate constant of a redox reaction, but also the electrode porosity [410].

The PEDOT-GO/GCE electrode shows larger I_{pa} & I_{pc} values of 80.48 μA and 88.19 μA respectively compared to that of bare GCE, which may be attributed to enhanced electroactive properties of GCE after deposition of PEDOT-GO composite [394]. After deposition of AuNPs to the composite film of PEDOT and GO, the ΔE_p values decrease from 109mV to 88 mV. Excellent conductivity of AuNPs [413] results in remarkable enhancement in peak current values I_{pa} and I_{pc} to 120 μA and 124 μA, respectively ($I_{pa}/I_{pc} \sim 0.96$). These results show that the catalytic activity of AuNPs/PEDOT-GO/GCE is excellent towards the redox reaction of Fe(IV)/Fe(III). The hybrid can enhance rapid electron transfer due to high conductivity of AuNPs providing plenty of electro-active sites that may be available due to large surface to volume ratio of AuNPs [414]. After immobilization of antibody and enzyme, the electron transfer between $[Fe(CN)_6]^{3-/4-}$ solution and the electrode decreases resulting in decrease in the peak current (Figure 5.5 (C)), since the antibody partially blocks the active sites after the covalent linkages of anti-AFB_1 and AChE with AuNPs/PEDOT-GO film.

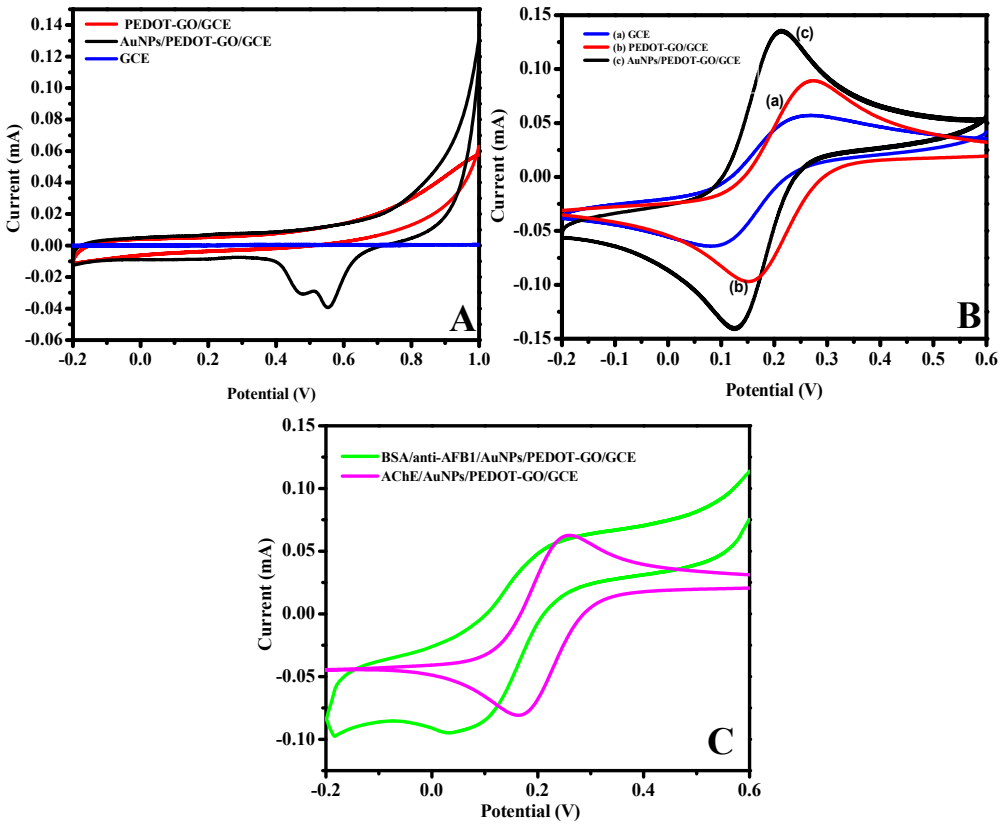

Figure 5.5: The CV patterns of bare (A) GCE, PEDOT-GO/GCE, AuNPs/PEDOT-GO/GCE in 100mM PBS (pH 7.4). (B) The CV of Bare GCE, PEDOT-GO/GCE, AuNP/PEDOT-GO/GCE and (C) The CV of BSA/anti-AFB_1/AuNPs/PEDOT-GO/GCE and AChE/AuNPs/PEDOT-GO/GCE in 100mM PBS (pH 7.4) and 5mM $[Fe(CN)_6]^{3-/4-}$ at 20 mV/s.

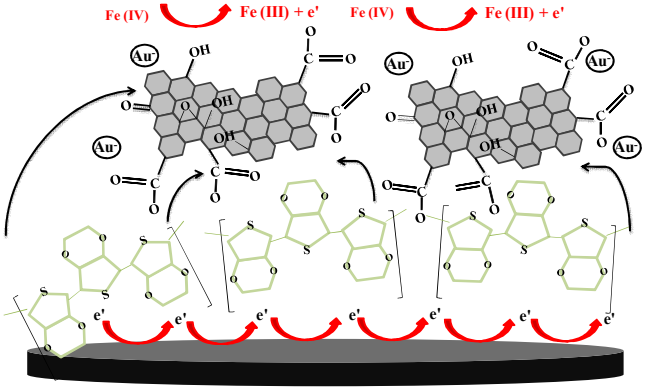

Scheme 5.1: The schematic representation of the electro-catalytic behavior of the modified electrode towards redox probe ($[Fe(CN)_6]^{3-/4-}$).

Table 5.2: The parameters of cyclic voltammogram (I_{pa}, I_{pc} and ΔE_p) for the modified electrodes.

Electrodes	I_{pa}	I_{pc} (-ve)	ΔE_p (E_{pa}-E_{pc}) mV)
GCE	54.6µA	57.12µA	135
PEDOT-GO/GCE	86µA	96µA	116
AuNPs/PEDOT-GO/GCE	135.7µA	153µA	92
BSA/anti-AFB1/AuNPs/PEDOT-GO/GCE	54.47µA	63.9µA	212
AChE/AuNPs/PEDOT-GO/GCE	62 µA	78 µA	142

5.6.2 Variation of Anodic (I_{pa}) and Cathodic Current (I_{pc}) vs. scan rate (v):

Figure 5.6 shows the variation of CV pattern of all the electrodes at different scan rate ranging from 5 mVs^{-1} to 30 mVs^{-1} and the variation follows an outer extension of all the peaks. The total current in cyclic voltammetry is sum total of faradaic current and the capacitive current; former is independent of the scan rate while the later increases with it [237, 238]. In order to find out the electrode mechanism, changing scan rate during cyclic voltammetry has been performed and all the electrodes show a linear variation of anodic and cathodic peak currents (I_{pa} & I_{pc}) with the square root of scan rate ($\upsilon^{1/2}$) (Figure 5.7). According to Randles-Sevcik [237, 238] expression direct proportionality of peak currents with the scan rate illustrates that the redox reaction is diffusion controlled process on the surface of the electrodes, suggesting no specific interaction between Fe(IV)/Fe(III) redox couple and electrodes. The linear regression equations of the electrode (1) PEDOT-GO/GCE, (2) AuNPs/PEDOT-GO/GCE, are given in equation (5.5 and 5.6) and the values of slopes and regression coefficient are tabulated in Table 5.3.

$$I_{pa}(mA) = 0.66 \times v^{\frac{1}{2}} + 0.01\ ;\ I_{pc}(mA) = -0.65 \times v^{\frac{1}{2}} + (-0.06); \qquad (5.5)$$

$$I_{pa}(mA) = 0.84 \times v^{\frac{1}{2}} + 0.027\ ;\ I_{pc}(mA) = -0.88 \times v^{\frac{1}{2}} + (-0.013); \qquad (5.6)$$

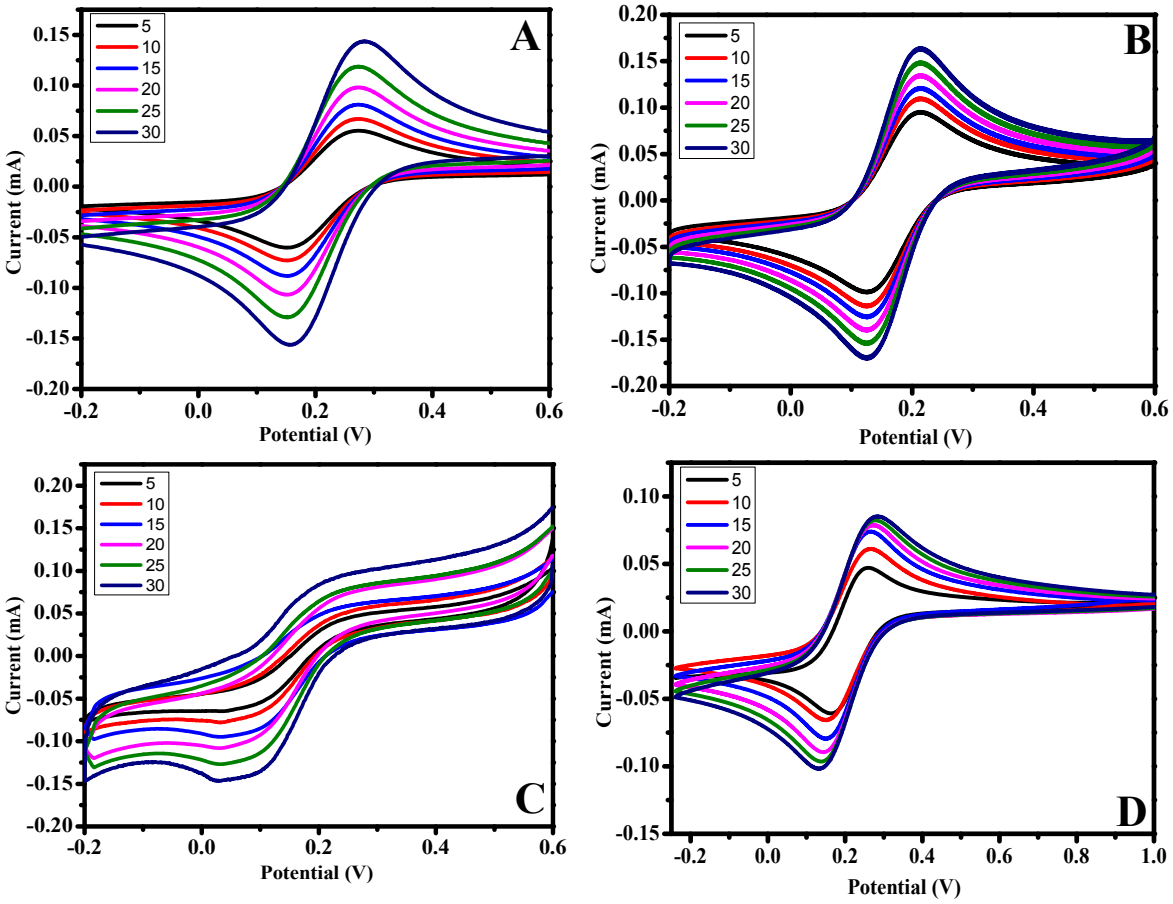

Figure 5.6: The Cyclic Voltammogram of (A) PEDOT-GO/GCE (B) AuNPs/PEDOT-GO/GCE, (C) BSA/anti-AFB_1/AuNPs/PEDOT-GO/GCE and (D) AChE/AuNPs/PEDOT-GO/GCE in 100mM PBS (pH 7.4) and 5mM $[Fe(CN)_6]^{3-/4-}$ at a scan rate ranging from 5 mV/s to 30 mV/s.

The electro-active areas can also be estimated based on the slope of the different electrodes using equation [240]:

$$A = \frac{Slope}{((2.69 \times 10^5 \times n^{\frac{1}{2}} \times D^{\frac{1}{2}} \times C))} \quad (5.7)$$

where A is the effective surface area, 'n' is the number of electron transferred, D is the diffusion coefficient and C is the concentration of redox species [240]. The calculated value of surface area for GCE, PEDOT-GO/GCE, AuNPs/PEDOT-GO/GCE has been tabulated in Table 5.4 and Au nanoparticles greatly increase the surface area, which is over 3 times higher than that of the GCE, making the AuNPs/PEDOT-GO/GCE is a good interface for antibody immobilization.

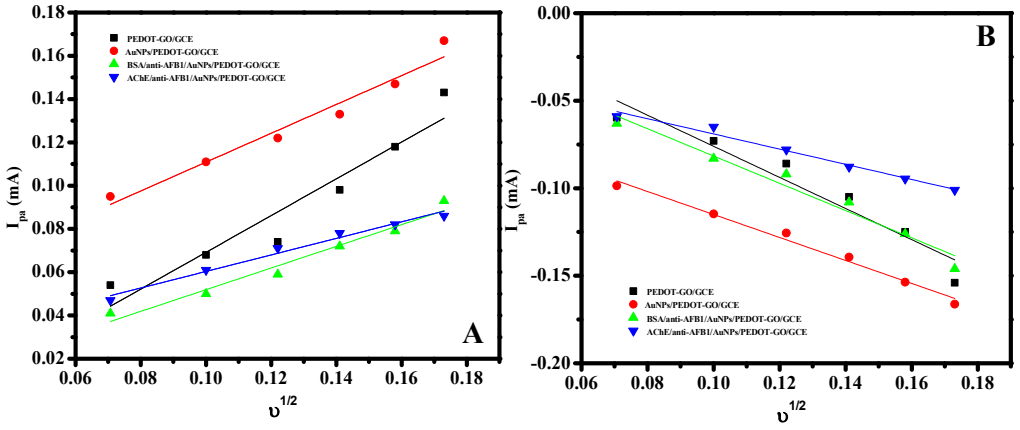

Figure 5.7: The variation of I_{pa} and I_{pc} of AuNPs/PEDOT-GO/GCE, PEDOT-GO/GCE, BSA/anti-AFB_1/AuNPs/PEDOT-GO/GCE and AChE/AuNPs/PEDOT-GO/GCE in 100mM PBS and 5mM $[Fe(CN)_6]^{3-/4-}$ with $\nu^{1/2}$ in V/s.

Table 5.3: The value of anodic and cathodic slope of all the modified electrodes:

Electrode	Anodic Slope	Cathodic Slope	Regression coefficient
PEDOT-GO/GCE	0.66	0.65	0.988
AuNPs/PEDOT-GO/GCE	0.84	0.88	0.981
BSA/anti-AFB1/AuNPs/PEDOT-GO/GCE	0.51	0.62	0.978
AChE/AuNPs/PEDOT-GO/GCE	0.39	0.43	0.974

Table 5.4: The calculated values of electro active surface area of the modified electrode.

Electrode	Electro-active area (cm^2)
GCE	0.08
PEDOT-GO/GCE	0.11
AuNPs/PEDOT-GO/GCE	0.235

The value of slope can further be used to estimate the total surface concentration (I^*) of the ionic species. The surface concentration (I^*) of the ionic species on the surface of BSA/anti-AFB_1/AuNPs/PEDOT-GO/GCE and AChE/AuNPs/PEDOT-GO/GCE have been estimated using the equation $I_p = \frac{n^2F^2I^*A\upsilon}{4RT}$, [248] where I^* is the estimated value of surface coverage of bioelectrodes in mol cm^{-2}; I_p/v can be calculated from the slope of Figure 5.8. The calculated value surface coverage of anti-AFB_1 and AChE over the surface of AuNPs/PEDOT-GO/GCE and PEDOT-GO/GCE has been tabulated in Table 4.5. The value of I^* is found to be more in AuNPs modified matrix as the spherical nanoparticle not only provides large surface area but also helps in immobilization of the protein as discussed in chapter 3 [392].

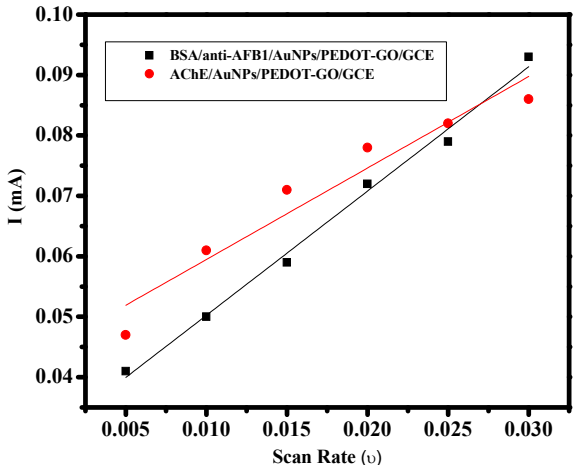

Figure 5.8: The linear variation of peak current (I_p) of BSA/anti-AFB_1/AuNPs/PEDOT-GO/GCE and AChE/AuNPs/PEDOT-GO/GCE versus ν in V/s.

Table 5.5: The value of ionic species after immobilization anti-AFB_1 and AChE.

Protein	Surface concentration (*I**) in PEDOT-GO/GCE ($molcm^{-2}$)	Surface concentration (*I**) in AuNPs/PEDOT-GO/GCE ($molcm^{-2}$)
anti-AFB_1	8.3×10^{-7}	2.3×10^{-5}
AChE	2.7×10^{-7}	3.15×10^{-5}

5.6.3 Variation of Anodic (E_{pa}) and Cathodic (E_{pc}) peak potential vs. Scan rate (v):

The effect of variation of scan rate (50 mV/s to 75 mV/s) on the position of the anodic peak potential (E_{pa}) and cathodic peak potential (E_{pc}) has been studied and in order to calculate the heterogeneous rate transfer constant (k_s) of the modified electrodes, we have plotted E_{pa} and E_{pc} with Log (υ) as shown in Figure 5.9. According to Laviron's method [254], the slopes of the E_{pa} and E_{pc} vs. Log (ν) can be used to calculate the transfer coefficient (α) and heterogeneous electron transfer constant (k_s) according to the following relation:

$$E_{pc} = E^0 + A\, ln\left[\frac{(1-\alpha)}{m}\right] \quad (5.8)$$

$$E_{pa} = E^0 + B\, ln\left[\frac{(\alpha)}{m}\right] \quad (5.9)$$

for $\Delta E_p > \frac{200(mV)}{n}$

$$logk_s = \alpha log(1-\alpha) + (1-\alpha) log\alpha - log\frac{Rt}{n\nu F} - \frac{\alpha(1-\alpha)nF\Delta E_p}{2.3RT} \quad (5.10)$$

where $A = \frac{RT}{(1-\alpha)nF}$, $B = \frac{RT}{\alpha nF}$

where *n* is the electron transfer number, R is the gas constant, T is the absolute temperature, and ΔE_p is the peak-to peak separation.

The smaller value of k_s value for AuNPs/PEDOT-GO/GCE indicates fast kinetics of the redox couple which may be attributed to the highly conducting nature of metal nanoparticles [413]. As presented in Table 5.6, the value of k_s falls in the quasi reversible mechanism range of $0.020 > k_s > 5 \times 10^{-5}$. The value of k_s of BSA/anti-AFB_1/AuNPs/PEDOT-GO/GCE and AChE/PEDOT-GO/GCE is found to

be 6.8×10^{-2} s^{-1} and 1.43×10^{-3} s^{-1}, respectively. It suggests that the electron transfer pathway of the protein behaved as a quasi-reversible system. Therefore we can consider AuNPs/PEDOT-GO/GCE as a suitable electrode for immobilization of protein to achieve better performance with improved sensitivity. The variation of peak to peak separation (E_{pa}-E_{pc}) with respect to the scan rate is an important parameter to understand electrode mechanism as discussed in section 2.2 in chapter 2. Figure 5.10 illustrates the linear variation of ΔE_p of all the modified electrodes with the scan rate showing a quasi reversible electrode mechanism [243].

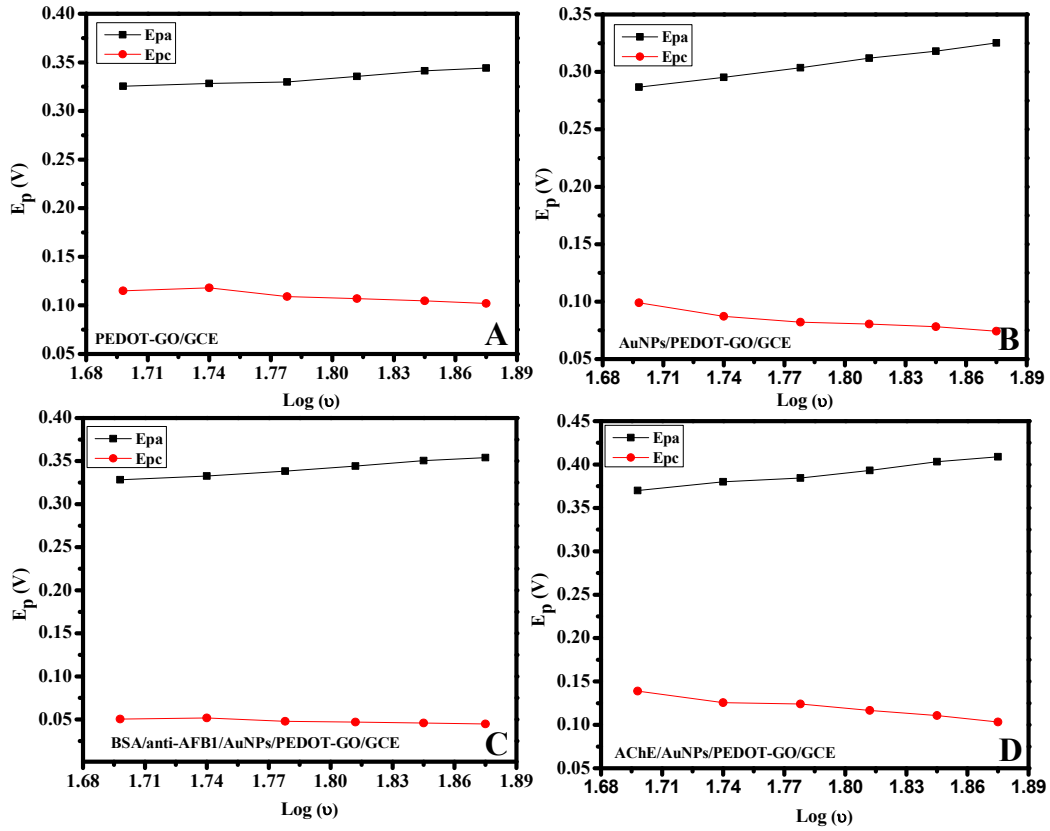

Figure 5.9: The variation E_{pa} & E_{pc} of (A) PEDOT-GO/GCE, (B) AuNPs/PEDOT-GO/GCE, (C) BSA/anti-AFB1/AuNPs/PEDOT-GO/GCE, (D) AChE/ AuNPs/PEDOT-GO/GCE w.r.t Log (ν) (50 to 75 mV/s).

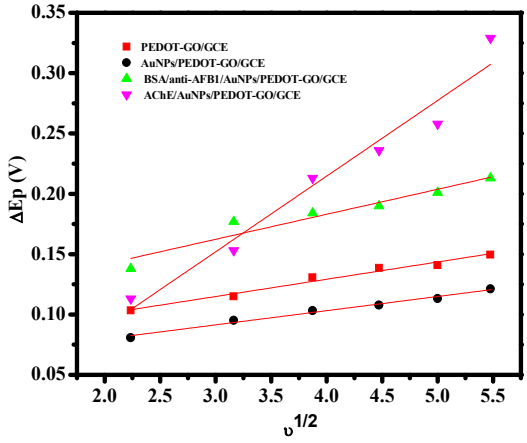

Figure 5.10: The variation ΔE_p of PEDOT-GO/GCE, AuNPs/PEDOT-GO/GCE, BSA/anti-AFB_1/AuNPs/PEDOT-GO/GCE, AChE/AuNPs/PEDOT-GO/GCE with $\nu^{1/2}$ in mV/s.

Table 5.6: The calculated values of heterogeneous rate transfer constant (k_s) and transfer coefficient (α).

Electrode	k_s (s^{-1})	α ($\alpha_a + \alpha_c$)/2
PEDOT-GO/GCE	1.26×10^{-1}	0.59
AuNPs/PEDOT-GO/GCE	1.61×10^{1}	0.58
BSA/anti-AFB_1/AuNPs/PEDOT-GO/GCE	6.8×10^{-2}	0.62
AChE/AuNPs/PEDOT-GO/GCE	1.43×10^{-3}	0.66

After studying the electro-catalytic behavior, we have performed the sensing experiments of (A) BSA/anti-AFB_1/AuNPs/PEDOT-GO/GCE and (B) AChE/AuNPs/PEDOT-GO/GCE, respectively.

5.7 Application of BSA/anti-AFB_1/AuNPs/PEDOT-GO/GCE to detect AFB_1:

5.7.1 Optimization of Experimental parameters:

Before carrying out the sensing experiments, the parameters like stability of the working electrodes, pH of the PBS and Fe $[(CN)_6]^{3-/4-}$ solution and the incubation time of antigen-antibody interaction have been optimized.

5.7.1.1 Electrochemical stability of the BSA/anti-AFB$_1$/AuNPs/PEDOT-GO/GCE before and after immobilization:

The Cyclic Voltammetry studies of AuNPs/PEDOT-GO/GCE in 100mM PBS and 5mM $[Fe(CN)_6]^{3-/4-}$ at a scan rate of 20mV/s for 20 cycles have been done in order to monitor the electrochemical stability (Figure 5.11 (A)). The area of CV remains constant indicating no remarkable degradation up to 20 cycles which may be due to the stable composite of PEDOT and GO retaining 98% stability.

It is important to study the stability after immobilization of the anti-AFB_1 in order to confirm whether the decrease in current during immune reaction is due to interaction of antigen & antibody, not due to poor stability of the BSA/anti-AFB_1/AuNPs/PEDOT-GO/GCE. Figure 5.11 (B) shows the CV pattern of BSA/anti-AFB_1/AuNPs/PEDOT-GO/GCE in 100mM PBS and 5mM $[Fe(CN)_6]^{3-/4-}$ at scan rate of 10mV/s for consecutive 20 cycles. There is no decrease in the values of I_{pa} & I_{pc} and the difference in peak potential (ΔE_p) remains constant indicating the stability of the electrode towards redox reaction of Fe(IV)/Fe(III) and confirms the decrease in current during immune-reaction is due to antigen- antibody interaction.

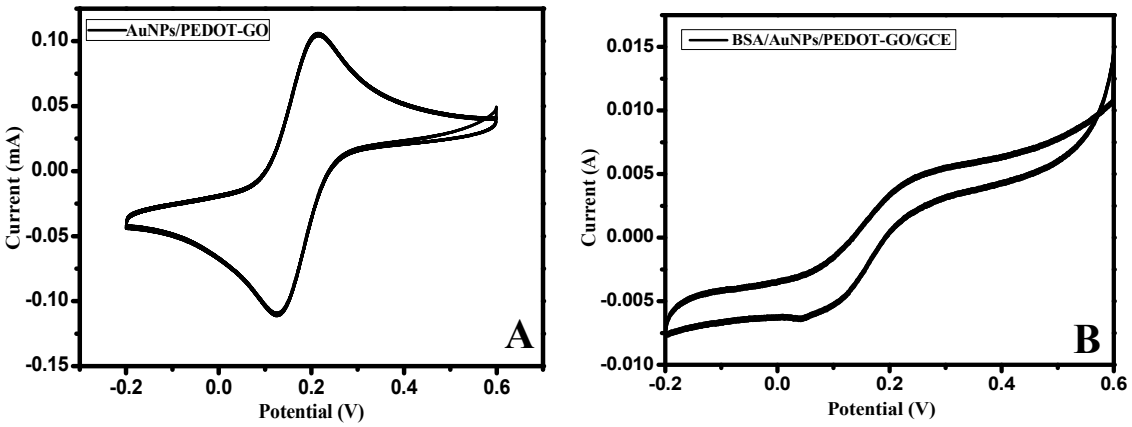

Figure 5.11: Cyclic voltammogram of (A) AuNPs/PEDOT-GO/GCE and (B) BSA/anti-AFB1/AuNPs/PEDOT-GO/GCE in 100 mM PBS and 5mM $Fe[(CN)_6]^{3-/4-}$ at 20 mV/s vs. Ag/AgCl.

5.7.1.2 Optimization of Immuno-assay conditions:

Many factors like pH of the operating electrolyte solution, concentration of methanol in dissolving AFB_1 and incubation time for immunoreactions play a vital role in the immune assay. Therefore, these factors have been optimized aiming to get an excellent sensitivity without affecting the structural confirmation of the antibodies. The Cyclic Voltammetry of the electrodes before immobilization (Figure 5.12(A)) has been studied at different pH ranging from 6.8 to 8.2. The sensitivity of the electrode towards the redox reaction of Fe(IV)/Fe(III) is found to be maximum for pH 7.4. In order to find out the optimum pH for the antigen sensing we performed DPV of the PEDOT-GO/GCE after immobilization of anti-AFB_1 as shown in Figure 5.12 (B) and maximum activity of anti-AFB_1 is found for pH 7.4. The corresponding EIS results have been depicted in Figure 5.12 (C), which are consistent with the DPV results.

The binding of the antigen and antibody results in increase in R_{et} value is also found to be maximum at pH 7.4 as DPV signal is minimum. This may be due to the fact that at low pH (highly acidic) and high pH (highly alkaline) environment, the antibodies may lose their binding ability [179]. The result implies that the interaction of immobilized AFB_1 with the immunospecies occurs more effectively at pH 7.4. It has been reported that the AFB_1 conjugated with anti-AFB_1 is partially redissolved in methanol [295] on the surface of the electrode which can be decremented from the antibodies binding site as the concentration of methanol exceeds 50%. The lower concentration of methanol (10%) was optimized for further experiments to remove any unfavorable condition during the immunoreactions.

The time required for the immune-reaction is important parameter to be optimized. Fig 5.13 (A) depicts that the DPV peak current change ΔI (I_0-I_i) increases gradually until 8 min and Fig 5.13 (B) shows variation of ΔI with time in minute. Thus 8 min was chosen as the optimized incubation time required for antigen and antibody interaction in the successive experiments. All the experiments were performed in room temperature.

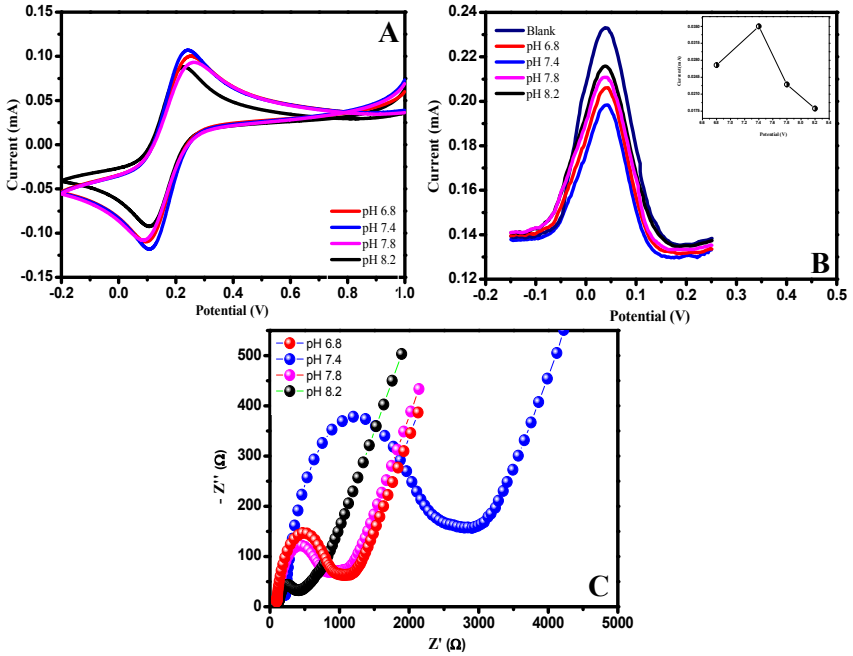

Figure 5.12: (A) The Cyclic voltammogram of AuNPs/PEDOT-GO/GCE (B) DPV studies of BSA/anti-AFB_1/AuNPs/PEDOT-GO/GCE (C) Nyquist Plot of BSA/anti-AFB_1/AuNPs/PEDOT-GO/GCE in a solution containing 100 mM PBS (pH 7.4) and 5mM $[Fe(CN)_6]^{3-/4-}$ with pH ranging from 6.8 to 8.2.

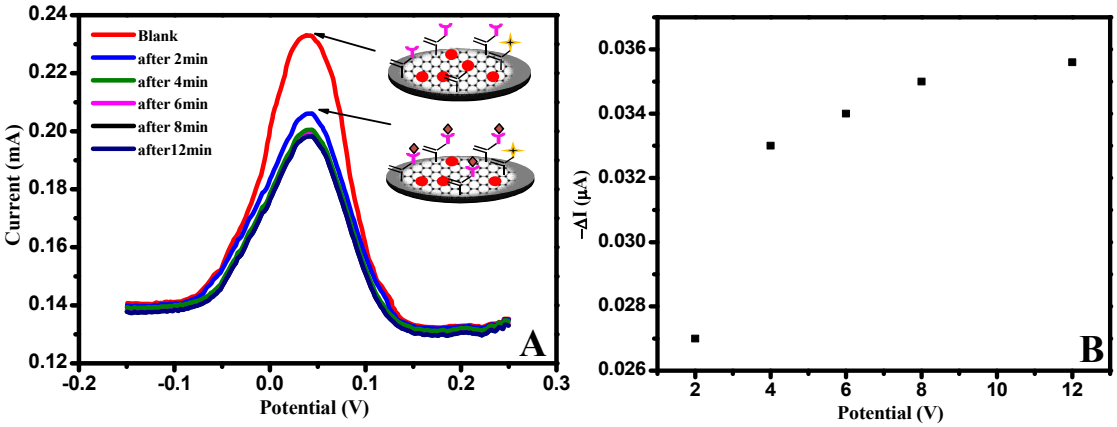

Figure 5.13: The variation of current in DPV of BSA/anti-AFB_1/AuNPs/PEDOT-GO/GCE in 100mM PBS (pH 7.4) and 5mM $Fe(CN)_6^{3-/4-}$ containing 20 ng/mL AFB_1 after different incubation time (B) The variation of ΔI with time in min.

5.7.2 Analytical Performance of the BSA/anti-AFB$_1$/AuNPs/PEDOT-GO/GCE:

The response of the immobilized anti-AFB$_1$ towards its immune-species is studied by performing DPV of BSA/anti-AFB$_1$/AuNPs/PEDOT-GO/GCE in 100mM PBS and 5mM $[Fe(CN)_6]^{3-/4-}$ in presence of different concentration of AFB$_1$. Figure 5.14 (A) shows the variation of current with the concentration of AFB$_1$ in the range of 0 to 90 ng/mL. The current decreases proportionally with increasing concentration of AFB$_1$ indicating effective binding of AFB$_1$ with the active site of anti-AFB$_1$. As mentioned earlier the antigen antibody interaction hinders the electron transfer between $[Fe\ (CN)_6]^{3-/4-}$ redox probe and the electrode [352]. The calibrated curve of ΔI (I_0-I_i) vs. concentration is shown in Figure 5.14 (B) shows a linear increase in ΔI at lower concentration and gradually a steady state is reached where no further increase in current was observed.

Linear response of BSA/anti-AFB$_1$/AuNPs/PEDOT-GO/GCE towards the detection AFB$_1$ is found in the two ranges of 0.5-20 ng/mL and 20-60 ng/mL as shown in Figure 5.15 (A & B) with regression equation of linearity plot of given by:

$$y = 0.998\ \mu A ng^{-1} mL\ \times (X) + 0.0169;\ R^2 = 0.9 \qquad 5.11$$

$$y = 0.397\ \mu A ng^{-1} mL\ \times (X) + 0.0211;\ R^2 = 0.9 \qquad 5.12$$

where y is the DPV peak current change (ΔI) in μA and X is AFB$_1$ concentration in ng/mL. This corresponds to the sensitivity of 0.998 μAng^{-1}mL within the linear range of 0.5-20 ng/mL and 0.397 μAngmL^{-1} within linearity range of 20-60 ng/mL, respectively. Figure 5.16 shows the calibration plot of maize samples spiked with AFB$_1$ with regression equation:

$$y = 11.8\ \mu A ng^{-1} mL\ \times (X) + 0.0167;\ R^2 = 0.99 \qquad 5.13$$

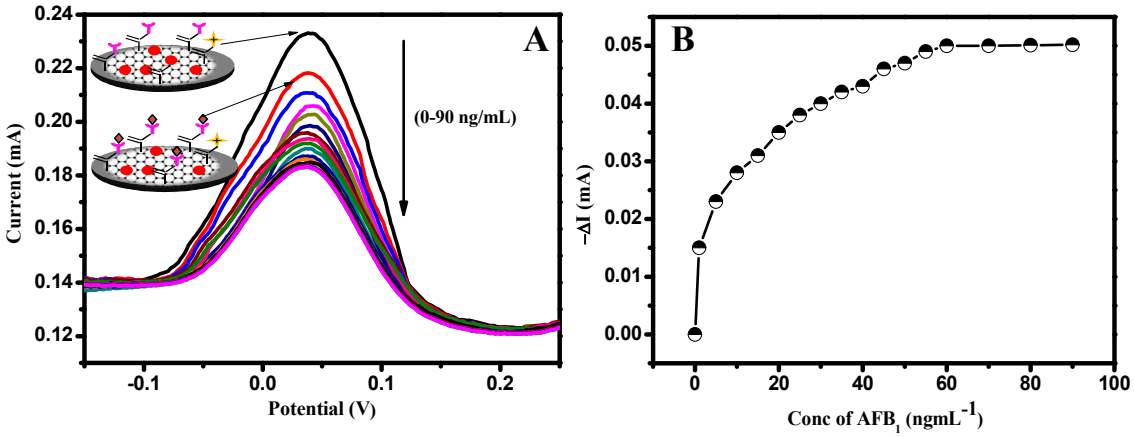

Figure 5.14: The DPV pattern of BSA/anti-AFB_1/AuNPs/PEDOT-GO/GCE with concentration of AFB_1 (0-90 ng/mL) in 100 mM PBS (pH 7.4) and 5 mM $[Fe(CN)_6]^{3-/4-}$. (B) The calibration plot of change in current (ΔI) vs. concentration in ng/mL.

This corresponds to the sensitivity of 11.81 $\mu A ngmL^{-1}$ towards spiked maize sample within the linear range of 0.1-1.81 $ngmL^{-1}$ .The limit of detection (LOD) and the limit of quantification (LOQ) were calculated from the parameters obtained from the regression curve, using LOD=3*S_y/s and LOQ=10*S_y/s, where 'S_y' is the standard deviation of the y-intercept and's' is the slope. The analytical parameters of the synthesized electrode towards its analyte are presented in Table 5.6

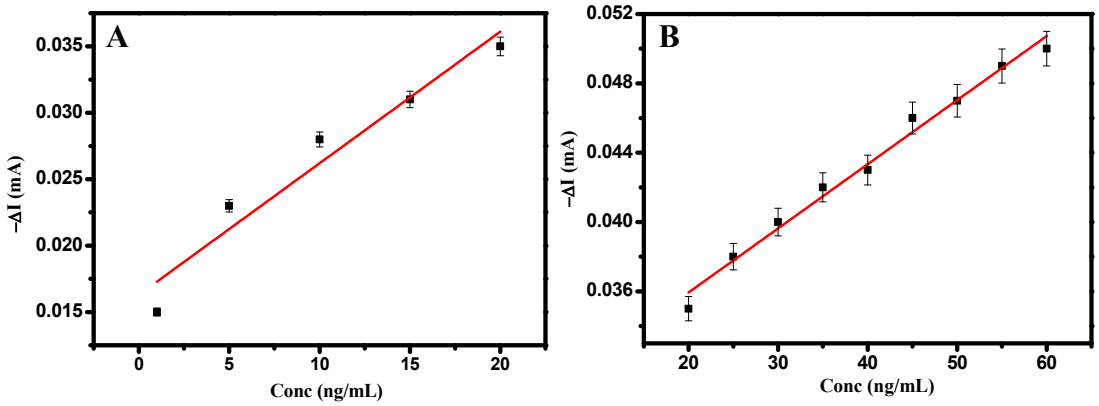

Figure 5.15: Linear slope of ΔI vs. Concentration in ng/mL of BSA/anti-AFB_1/AuNPs/PEDOT-GO/GCE towards AFB_1.

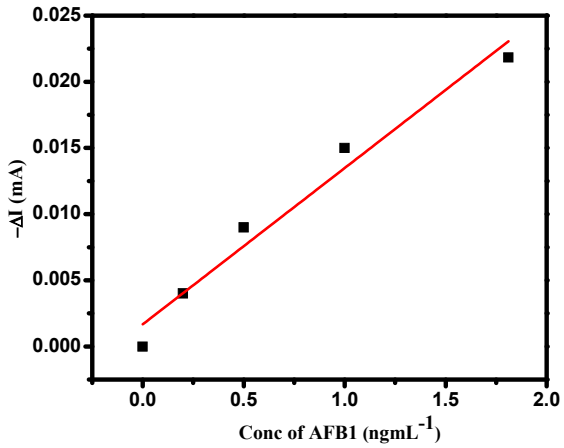

Figure 5.16: The linear response of the BSA/anti-AFB_1/AuNPs/PEDOT-GO/GCE in varying concentration of AFB_1 in maize matrix.

Table 5.7: Analytical Parameters of the fabricated electrode towards the detection of AFB_1 in PBS and maize matrix.

Parameters	Values (in PBS)	Values (in maize matrix)
Linearity range (ng/ml)	0.5 to 20 ng/mL and 20 to 60 ng/mL	0.1 to 1.81 ng/mL
Sensitivity	0.998 μAng-^{1}mL and 0.378 μAng-^{1}mL	11.81 μAng-^{1}mL
Correlation Coefficient (R^2)	0.98; 0.99	0.98
LOD	0.109 ng/mL	0.01 ng/mL
LOQ	0.377 ng/mL	0.0384 ng/mL

5.7.3 Specificity and recovery of BSA/anti-AFB_1/AuNPs/PEDOT-GO/GCE towards real sample:

In order to validate the feasibility of the synthesized electrochemical immunosensor to detect AFB_1 specifically, AFB_1 spiked corn samples were analyzed. The DPV results of BSA/anti-AFB_1/AuNPs/PEDOT-GO/GCE in presence of corn sample spiked with 20 ng/mL and 40 ng/mL of AFB_1 have been displayed in Figure 5.17, respectively. The statistical calculation of standard addition method of spiked and

unspiked samples is tabulated in Tables 5.7 and 5.8. The measured average recoveries % $\left[\frac{measured\ value}{expected\ value} \times 100\right]$ is in the range of 92.18% and 95.4 % for 20 ng/mL and 40 ng/mL concentration of AFB_1, respectively. The results suggest that the immunoelectrode is capable of detecting AFB_1 in real corn sample without any interference or cross reactivity indicating specificity of BSA/anti-AFB_1/AuNPs/PEDOT-GO/GCE electrode. Thus the electrode meets the requirement of ultra-sensitive detection of AFB_1.

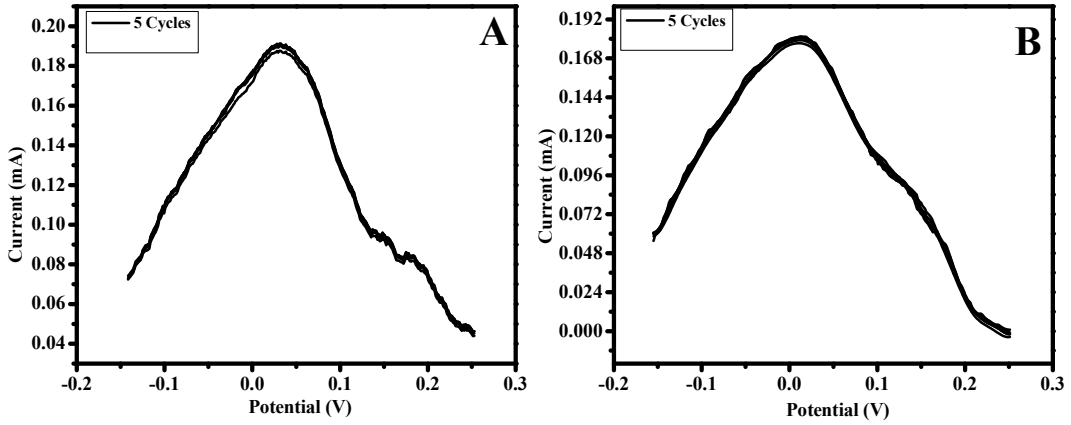

Figure 5.17: The DPV current variation of peak current of BSA/anti-AFB_1/AuNPs/PEDOT-GO/GCE in 100mM PBS (pH 7.4) and 5mM $Fe(CN)_6^{3-/4-}$ containing real corn sample spiked with (A) 20 ng/mL and (B) 40 ng/mL, respectively.

Table 5.8: Statistics and performance characteristics of the working electrodes towards s tandard AFB_1 sample.

Concentration of Aflatoxin B_1	Measured Current (mA)	Average (x)	SD	RSD (%)
20 ng/ml	0.202	0.209	0.005715	2.734678
	0.212			
	0.209			
	0.214			
	0.201			
40 ng/ml	0.191	0.19	0.002	0.789639
	0.191			
	0.187			
	0.189			
	0.192			

Table 5.9: Statistics and performance characteristics of the working electrodes towards standard spiked AFB_1 sample.

Concentration of Aflatoxin B_1 Spiked (Conc of spiked/ standard AFB_1) (1:3)	**Measured Current (mA)**	**Average (x)**	**SD**	**RSD (%)**
20 ng/ml	0.191	0.19072	0.001533623	0.804123
	0.190			
	0.189			
	0.193			
	0.190			
40 ng/ml	0.181			
	0.180			
	0.179			
	0.188			
	0.180	0.182	0.003437	1.88

5.8 Application of AChE/AuNPs/PEDOT-GO/GCE to detect Organophosphate (methyl parathion):

5.8.1 Analytical behavior of AChE/AuNPs/PEDOT-GO/GCE towards Acetylthiocholine Chloride (AThCl):

The detection of methyl parathion is based on the study of the inhibition of AChE activity towards its analyte, thiocholine in presence of methyl parathion. The enzymatic behavior AChE immobilized on the matrix of AuNPs/PEDOT-GO/GCE towards acetylthiocholine chloride (AThCl) has been studied using cyclic voltammetry. The reaction in presence of AChE can be described by the following equations:

$$Acetylthiocholine\ chloride \xrightarrow{AChE} thiocholine + acetic\ acid$$

$$Thiocholine\ (red) \rightarrow disulfide\ (Ox) + 2H^+ + 2e^- \qquad 5.14$$

The immobilized AChE will breakdown AThCl into thiocholine which will get oxidized and it appears as the oxidation peak in cyclic voltammogram. Figure 5.18

shows the cyclic voltammogram pattern of AChE/AuNPs/PEDOT-GO/GCE in absence (curve a) and in presence of different concentration of AThCl. In absence of AThCl there is no visible peak current which indicates no redox activity of AChE in PBS. An oxidation peak current of intensity 0.031 mA at 0.8 V vs. Ag/AgCl was observed which is due to oxidation of thiocholine (RSH) (equation 5.14) [396].A reduction peak at around -0.35 V is due to the reduction of RSSR which is produced during anodic oxidation of thiocholine [369]. The oxidation peak current increases with increasing concentration of AThCl which implies increase affinity of the immobilized AChE in presence of analyte. The effect of scan rate on the catalytic behavior of the enzyme electrode towards its analyte has been studied and it is displayed in Figure 5.19 (A). The diffusion coefficient of thiocholine has been calculated from the slope of linear plot of anodic current with the scan rate. The linearity in the variation of oxidation current with the scan rate indicates a diffusion controlled process of thiocholine species.

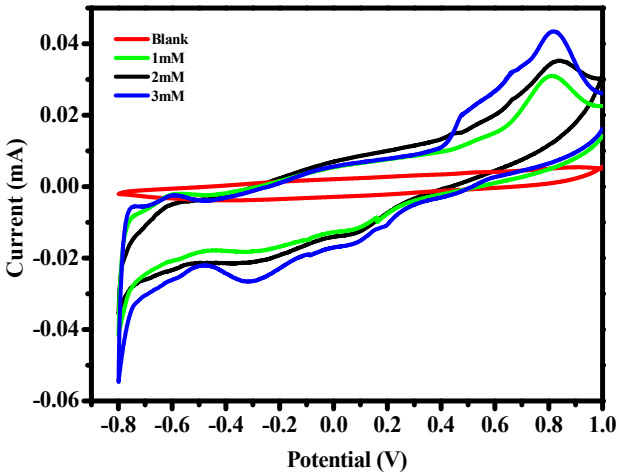

Figure 5.18: The cyclic voltammogram of AChE/AuNPs/PEDOT-GO/GCE in 100mM PBS in absence and presence of different concentration of AThCl at a scan rate of 5mV/s vs. Ag/AgCl.

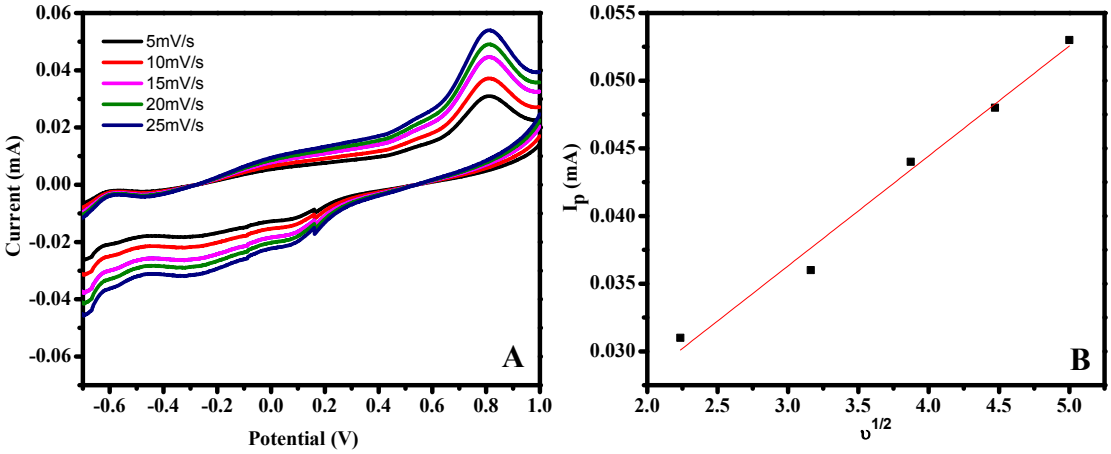

Figure 5.19: (A) The cyclic voltammogram of AChE/AuNPs/PEDOT-GO/GCE in 100mM PBS and 2mM AThCl at different scan rate and (B) Linear variation of peak current (I_{pa}) vs. square root of scan rate ($\nu^{1/2}$).

Figure 5.20 (A) shows the DPV pattern of AChE/AuNPs/PEDOT-GO/GCE in 100mM PBS in varying concentration of AThCl ranging from 0.1 mM to 10 mM. The enzyme electrode shows Michaelis Menten behavior as the intensity of the peak current increases initially with increasing concentration of AThCl and saturation of enzyme activity occurs. Figure 5.20 (B) shows the calibration plot of the oxidative amperometric signal of the AChE/AuNPs/PEDOT-GO/GCE vs. concentration of AThCl and the Figure 5.20 (C) is the Lineweaver Burk plot. The value of Michaelis Menten constant K_m has been calculated from lower linear part of calibration plot using equation 5.13 [266]:

$$\frac{1}{i} = \frac{1}{I_{max}} + \frac{K_m}{I_{max}[AThCl]} \qquad 5.15$$

where I_{max} corresponds to the maximum current of thiocholine oxidation where saturation occurs.

The value of K_m was found to be 0.2 mM which is lower than the K_m value (0.8 mM) for AuNPs/PEDOT/GCE system which implies better activity of AChE in AuNPs/PEDOT-GO/GCE. Similarly the maximum current towards the detection of thiocholine is found to be 255 µA. This is may be attributed to more immobilization of AChE over the matrix of AuNPs/PEDOT-GO/GCE which may be due to the presence of comparatively smaller size of AuNPs and the functional bonds of GO which form covalent bond with the NH_2 group of the enzyme [392].

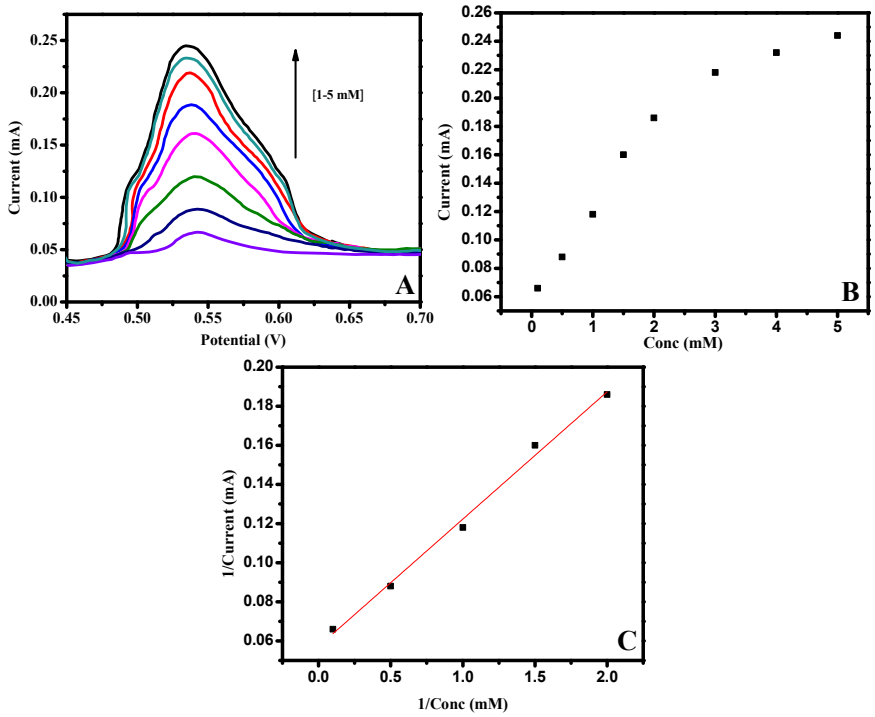

Figure 5.20: (A) The DPV pattern of AChE/AuNPs/PEDOT-GO/GCE in 100mM PBS and in presence of different concentration of 0.1 mM to 5 mM AThCl and (B) Calibration plot and (C) Lineweaver Burk Plot.

5.8.2 Inhibition AChE/AuNPs/PEDOT-GO/GCE in presence of methyl parathion:

The electrochemical detection was based on the measuring the response of the AChE/AuNPs/PEDOT-GO/GCE in 100 mM PBS and 2 mM AThCl and the increase in current with respect to the base current was considered as (I_0). After that, the bioelectrode was kept for the respective optimized time in the solution containing different pesticides samples and the corresponding response was considered as I_i.

The percentage of Inhibition (I %) and residual enzyme activities were calculated using equations (5.16 & 5.17) [415, 416] :

$$Inhibition\ \%\ (I\%) = [(\frac{I_0 - I_i}{I_0}) \times 100 \quad (5.16)$$

$$Residual\ enzyme\ activity\ \%\ (REA\ \%) = \left[\frac{I_i}{I_0}\right] \quad (5.17)$$

Figure 5.21 shows the DPV peak current variation of the AChE/AuNPs/PEDOT-GO/GCE in 100mM PBS and 2 mM AThCl in absence and in presence of varying concentration of methyl parathion ranging from 1 ng/mL to 50 ng/mL after 8 min incubation. It is evident that the DPV peak current decreases gradually with the increase of concentration of methyl parathion. There is a noticeable decrease in the peak intensity after incubation with methyl parathion which can be explained by the decrease in the activity of AChE due to formation of enzyme-inhibitor complex. It results in the less or non-availability of AChE to react with AThCl and this leads to less or no production of thiocholine and hence decreased in the current [417].

The effect of inhibition has been further investigated by plotting I% vs. concentration of methyl parathion and calibration curve shows an increase in the inhibition of enzyme activity with increasing concentration of methyl parathion and finally saturation occurs. The AChE/AuNPs/PEDOT-GO/GCE shows linearity in two ranges 1-15 ng/mL and 20-35 ng/mL with regression equation of $I(\%) = 2.60\,[x] + 2.579$ and $I(\%) = 1.157\,[x] + 30.9$ (Figure 5.22).

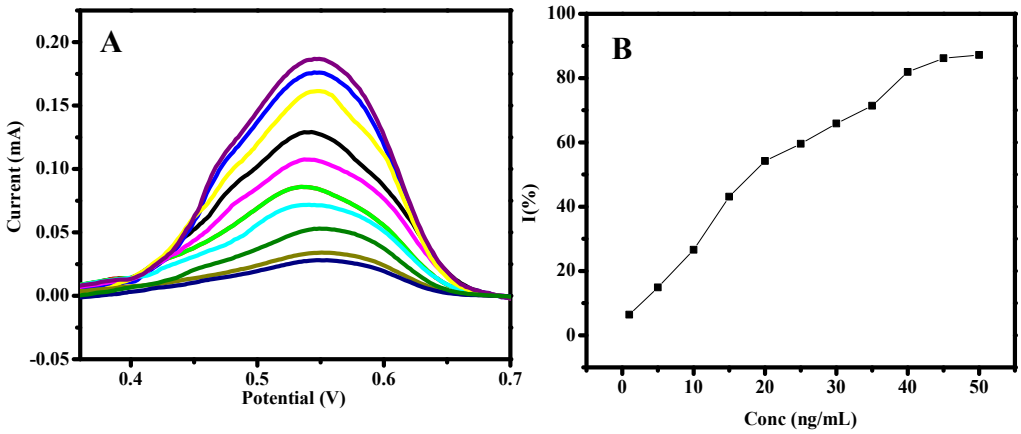

Figure 5.21: The DPV pattern of AChE/AuNPs/PEDOT-GO/GCE in 100mM PBS and 2mM of AThCl in different concentration of MP and (B) Calibration curve of I (%) with concentration in ng/mL.

The results indicate that the bioelectrode AChE/AuNPs/PEDOT-GO/GCE is an efficient sensor for the detection of the individual pesticides. The response is further studied by determining the limit of detection (LOD) and limit of quantification (LOQ) using the relation $3\times S_0/S$ and $10\times S_0/S$, where S_0 is the slope of the

calibration plot taken for minimum concentration of the pesticide sample. The analytical parameters towards the response of methyl parathion have been tabulated in Table 5.9 respectively.

After inhibition, the residual activity of the enzyme in AuNPs/PEDOT-GO/GCE decreases as the pesticides sample concentration increases (Figure 5.23). The immobilized enzyme retains 54.8% of its activity after the pesticides inhibition. The shelf life of the AChE/AuNPs/PEDOT-GO/GCE electrode has been studied and found that the biosensor showed a good activity and after weekly usage till 140 days the bioelectrode showed recovery of 91% when storage in phosphate buffer at 5^0C.

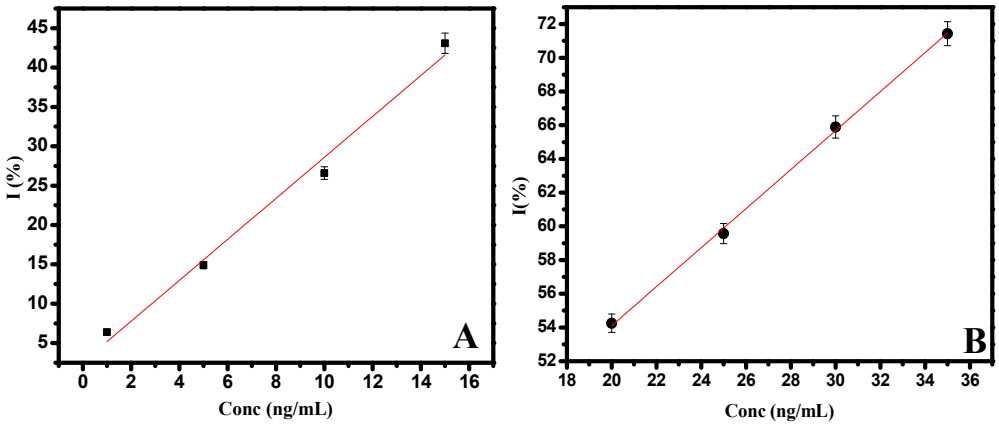

Figure 5.22: The linear response of AChE/AuNPs/PEDOT-GO/GCE towards the detection of MP.

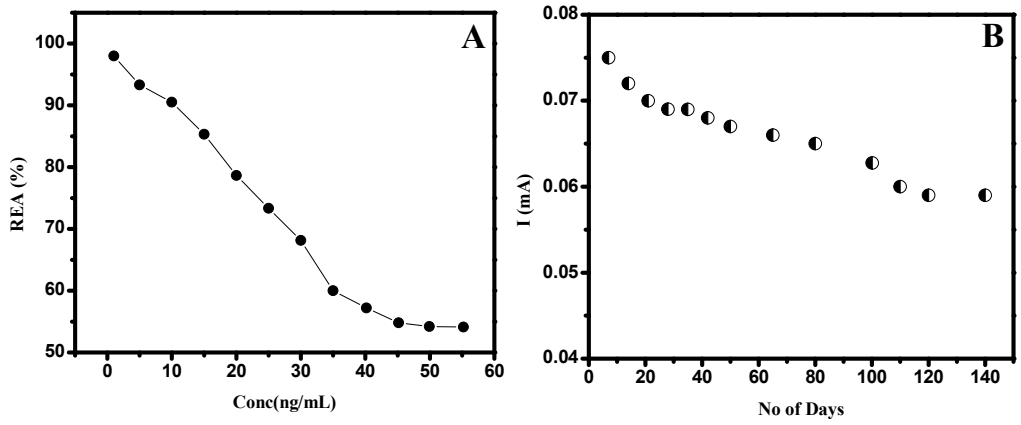

Figure 5.23: (A) Residual enzyme activity percentage (REA %) of AChE after methyl parathion inhibition and (B) Shelf life study of the immobilized AChE and its activity towards AThCl

Table 5.10: Analytical parameters of AChE/AuNPs/PEDOT-GO/GCE towards the detection of MP.

Parameters	Towards Methyl Parathion
Linearity (ng/mL)	0.1-15 ng/mL; 20-45 ng/mL
Sensitivity	2.60 $(ng/mL)^{-1}$ 1.57 $(ng/mL)^{-1}$
Correlation Coefficient (R^2)	0.95; 0.99
LOD	0.14 ng/mL
LOQ	0.470 ng/mL

5.9 Summary:

PEDOT-GO and PEDOT-GO functionalized with Au-NPs have been synthesized electrochemically and their morphological, surface properties and electrochemical activities have been investigated. FESEM micrograph confirms that the thickness of graphene oxide sheets is 12 to 15 nm and the spherical AuNPs of average size 45 nm to 56 nm are uniformly distributed on the petal like surface of PEDOT-GO onto which anti-AFB_1 and AChE have been immobilized using covalent coupling. The PEDOT-GO matrix provides an ideal platform for the non agglomerated deposition of AuNPs of average size ca. 50 nm, whereas comparatively larger nanoparticles of size 200- 300 nm have been deposited on PEDOT surface as presented in Chapter 4. The hydrophilic nature of GO and functionalization of PEDOT-GO/GCE matrix with Au-NPs result in decrease in contact angle to a value of 22^0 making the film more suitable for anti-AFB_1 and AChE immobilization. FTIR results show the characteristic bonding of different functional groups in PEDOT, GO and the conformational binding of AChE and anti-AFB_1 with the AuNPs/PEDOT-GO/GCE matrix which demonstrate the successful immobilization of the biomolecules. The R_{et} value of the functionalized electrode AuNP/PEDOT-GO/GCE is found to be 105 Ω that has been used for the immobilization of anti-AFB_1 and AChE. The value of C_{dl} is maximum for BSA/anti-AFB_1/PEDOT-GO/GCE and AChE/AuNPs/PEDOT-GO/GCE with phase angle of 78.4^0 and 60^0 indicating that the AuNPs/PEDOT-GO electrode becomes more capacitive after immobilization of anti-AFB_1 and AChE which are non-conducting in nature. Two reduction peaks at 0.45 V and 0.546 V

appeared for AuNPs/PEDOT-GO/GCE in PBS, corresponding to the reduction reactions of Au(3+)→Au(+) and Au(+)→Au(0), implying that Au nanoparticles are successfully deposited on the surface of the PEDOT-GO film. The cyclic voltammetry experiments performed in the redox solution and high peak current value of 136 μA and -153 μA (I_{pa} and I_{pc}) and the ΔE_p suggests an enhanced redox behavior of AuNPs/PEDOT-GO/GCE to Fe(IV)/Fe(III) and quasi reversible electrode mechanism. The electro-active surface area of AuNPs/PEDOT-GO/GCE is found to be 0.235 cm^2 which is higher than PEDOT-GO/GCE and GCE. Better immobilization of anti-AFB_1 and AChE occurs in AuNPs/PEDOT-GO/GCE as both carboxyl groups on the planes of GO and dative binding of AuNPs were involved in forming chemisorption covalent bond with the amine group of proteins. The surface coverage of anti-AFB_1 and AChE over AuNPs/PEDOT-GO/GCE was found to be 1.76×10^{-5} and 1.13×10^{-5} mol cm^{-2} which is higher than the value obtained AuNPs/PEDOT/GCE. This may be due the synergistic effect of spherical AuNPs and GO nanocomposite. The value of k_s falls in the quasi reversible mechanism range of $0.020> k_s > 5\times 10^{-5}$. The smaller k_s value for AuNPs/PEDOT-GO/GCE indicates fast kinetics of the redox couple that may be attributed to the highly conducting nature of metal nanoparticles. The electrochemical deposition of AuNPs/PEDOT-GO/GCE biocompatible film not only simplified the fabrication but also made the bioelectrode more sensitive and stable.

There is no decrease in the values of I_{pa} & I_{pc} and the difference in peak potential (ΔE_p) remains constant of the BSA/anti-AFB_1/AuNPs/PEDOT-GO/GCE indicating the stability of the electrode towards redox reaction of Fe(IV)/Fe(III) and confirms that the decrease in current during immuno-reaction is due to antigen-antibody interaction. The immunosensor shows maximum activity in a pH of 7.4 and the time required for the interaction with AFB_1 is optimized as 8 min. The synthesized immunosensor BSA/anti-AFB_1/AuNPs/PEDOT-GO/GCE exhibits high sensitivity of 0.989 $\mu Ang^{-1}mL$ towards AFB_1 concentration in linear range of 0.5-20 ng/mL with limit of detection (LOD) of 0.109 ng/mL and limit of quantification (LOQ) of 0.377 ng/mL. The sensitivity of BSA/anti-AFB_1/AuNPs/PEDOT-GO/GCE towards real maize sample has been performed and the electrode shows a linearity of 0.1-1.81 ng/mL with an excellent sensitivity of 11.81 $\mu Ang^{-1}mL$ with LOD of 0.09 ng/mL and LOQ 0.3 ng/mL.

The fabricated immunoelectrode BSA/anti-AFB1/AuNPs/PEDOT-GO/GCE shows a recovery of 92.25% and 95.79 % towards real maize sample spiked with AFB_1 of concentration 20 ng/mL and 40 ng/mL, respectively.

On the other hand the enzyme electrode AChE/AuNPs/PEDOT-GO/GCE shows good enzymatic activity and the oxidation of thiocholine occurs at 0.75 V vs. Ag/AgCl. An excellent affinity of the immobilized AChE towards AThCl was found with K_m value of 0.2 mM and I_{max} of 255 μA. The linearity in the variation of oxidation current with the scan rate indicates a diffusion controlled process of thiocholine species. The AChE/AuNPs/PEDOT-GO/GCE shows linearity in two ranges of 0.1-20 ng/mL and 30-40 ng/mL towards the inhibition of methyl parathion. The LOD and LOQ of the biosensor were found to be 0.14 ng/mL and 0.470 ng/mL. After inhibition, the residual activity of the enzyme in AuNPs/PEDOT-GO/GCE decreases as the pesticides sample concentration increases with time. The immobilized enzyme retains 54.8% of its activity after the pesticide inhibition. The AChE/AuNPs/PEDOT-GO/GCE shows a good activity and recovery of 91% after weekly usage till 140 days when storage in phosphate buffer at 5 ^{0}C.